RSC Advances

PAPER

View Article Online
View Journal | View Issue

Check for updates

Cite this: *RSC Adv.*, 2017, **7**, 32049

Multifunctional triple-porous Fe_3O_4@SiO_2 superparamagnetic microspheres for potential hyperthermia and controlled drug release†

Xuegang Lu,*[a] Qianru Liu,[b] Liqun Wang,[a] Wenfeng Jiang,[a] Wenying Zhang[a] and Xiaoping Song[a]

Magnetic porous particles with high magnetization and large surface area hold great potential for multimodal therapies. In this work, novel triple-porous Fe_3O_4@SiO_2 microspheres were synthesized by encapsulation of porous Fe_3O_4 with dual-porous SiO_2 shells. This novel triple-porous structure endows the microspheres with features of large surface area (426 m^2 g^{-1}) and pore volume; thus they could be used as an efficient drug delivery platform. These microspheres demonstrate superparamagnetic behavior with saturation magnetization of 52 emu g^{-1}. Measurements of AC magnetic-field-induced heating properties showed that the as-prepared microspheres could controllably generate heat to reach the hyperthermia temperature within a short time of exposure to an alternating magnetic field (AMF); hence they could be suitable as a hyperthermia agent for thermal therapy. Using a therapeutic agent 5-fluorouracil (5-Fu) as a model drug, the porous microspheres display high drug loading capacity, and sustained release behavior can be observed under the condition of no AMF actuation, while under the excitation of AMF, controlled drug release behavior can be achieved. Due to its magnetic field induced heating and AMF controlled drug release capabilities, this triple-porous nanomaterial provides an excellent platform for both hyperthermia treatment and drug delivery.

Received 21st January 2017
Accepted 12th June 2017

DOI: 10.1039/c7ra00899f

rsc.li/rsc-advances

Open Access Article. Published on 22 June 2017. Downloaded on 1/24/2026 4:51:22 AM.
This article is licensed under a Creative Commons Attribution 3.0 Unported Licence.

Introduction

Core–shell structured porous nanocomposites with functionalized interior cores and permeable outer shells have recently been recognized as ideal and powerful platforms for wide application in various fields.[1–7] Among these, core–shell structured microspheres consisting of a magnetic iron-oxide core and mesoporous silica shell have attracted particular attention owing to their unique magnetic response properties, low cytotoxicity, chemically modifiable surface, high surface areas, well-defined pore structures and multi-functionalities.[8–10] The magnetic response of iron-oxide cores enables them to be targeted, imaged and recycled.[11–13] Thus, they have been believed to be promising candidates for drug delivery platforms because they can carry drug molecules and can be magnetically guided to the targeted organs or lesion sites inside the body. Furthermore, these targeted magnetic materials at the tumor sites could be remotely heated by applying an alternating magnetic field (AMF), so that they could be used as magnetically controlled hyperthermia or thermoablation agents to generate localized heating for killing of cancer cells. On the other hand, the porous structures of silica materials endow them with high drug-loading capability and sustained release properties due to their high surface area, large pore volume and ease of surface functionalization. They have potential to be used as efficient drug carrier and sustained drug release platform. Therefore, the integration of porous silica with magnetic particles to form core@shell structures presents a good way for simultaneous hyperthermia treatment and drug delivery.[10,14–20] Combination of chemotherapy and hyperthermia would greatly improve the therapeutic effect against cancers.

In view of biological applications, the ideal magnetic material should possess quick magnetic response for fast separation, suitable surface area to maximize loading target objects and excellent biocompatibility to avoid any cytotoxic effect.[21–23] So far, many efforts have been made to achieve magnetic mesoporous silica microspheres.[24–26] However, most of these materials either show poor magnetic response, irregular core–shell structures, and single porous structure or possess mesopores that are difficult to access. This limits their performance in biomedical applications. To achieve quick magnetic response and good dispersion stability, superparamagnetic properties with high magnetization are needed. High magnetization enable easy separation or targeting of the particles by external

[a]MOE Key Laboratory for Non-equilibrium Synthesis and Modulation of Condensed Matter. School of Science, Xi'an Jiaotong University, Xi'an 710049, China. E-mail: xglu@mail.xjtu.edu.cn; Fax: +86 29 83237910; Tel: +86 29 82663034

[b]School of Physics & Information Technology, Shaanxi Normal University, Xi'an 710119, China

† Electronic supplementary information (ESI) available. See DOI: 10.1039/c7ra00899f

Open Access Article. Published on 22 June 2017. Downloaded on 1/24/2026 4:51:22 AM.
This article is licensed under a Creative Commons Attribution 3.0 Unported Licence.

magnetic fields, and superparamagnetism can prevent the particles from aggregating due to strong magnetic interactions in circulation.[27] Several methods have been developed to prepare superparamagnetic iron-oxide nanoparticles including thermal decomposition, reverse micelle synthesis, and solvothermal synthesis.[28–31] However, most of these superparamagnetic particles show low saturation magnetization owing to their small size (less than 20 nm). An increase in the size can increase the magnetization, unfortunately this may also induce the superparamagnetic–ferromagnetic transition. Therefore, how to achieve magnetic particles with both superparamagnetism and high saturation magnetization is still a challenge.

In addition, to achieve silica shells with desirable porous structure, many methods have been explored in controlling the permeation of silica shells. Various types of templates, such as cetyltrimethylammonium bromide (CTAB), *n*-octadecyltrimethoxysilane (C_{18}TMS), polyvinylpyrrolidone (PVP) *et al.* have been employed as porogens in creating mesoscale pores.[32–35] Disordered, highly ordered or even rattle-type mesoporous SiO_2 shells have been achieved. Unfortunately, these materials commonly possess single or monotonous porous structure so that it is difficult to obtain high surface area, high drug loading capacity and desirable drug release properties. To further achieve highly porous iron-oxide@SiO_2 nanocomposites, some new types of porous configurations have been proposed recently. For example, Ken Cham-Fai Leung *et al.* designed and successfully prepared dual-porous γ-Fe_2O_3@meso-SiO_2 microspheres using a templating method, in which porous γ-Fe_2O_3 cores were coated by porous SiO_2 shells. These dual-porous microspheres, with BET surface area about 222.3 $m^2\ g^{-1}$, can be used as a bifunctional agent for both MRI and drug carrier.[36] Haijiao Zhang *et al.* developed a multi-shelled mesoporous silica microsphere by a facile dual-templating method. The BET surface area and total pore volume was calculated to be 237.0 $m^2\ g^{-1}$ and 0.40 $cm^3\ g^{-1}$, respectively.[37] Guang Shao *et al.* developed a one-step electrostatic self-assembly templated approach to achieve yolk–shell structured Fe_3O_4@SiO_2 nanospheres with very high specific surface area, a huge cavity and ink-bottle type pores.[38] Although great efforts have been made in exploring new types of porous structures of iron-oxide@SiO_2 nanocomposites, it is still a great challenge to obtain iron-oxide@SiO_2 with more sophisticated pore configurations.

Herein, we report a facile synthesis route to obtain novel triple-porous Fe_3O_4@SiO_2 microspheres. First, mesoporous Fe_3O_4 cores (denoted as m-Fe_3O_4) are prepared through a modified hydrothermal method. Then, the Fe_3O_4 cores are coated by SiO_2 shells. By controlling the permeation of silica shells through "surfactant-templating and surface-protected etching" strategy, dual-porous SiO_2 shells (denoted as dm-SiO_2) are formed on the surface of porous Fe_3O_4 cores. As-made multiple-porous magnetic microspheres possess superparamagnetism and high magnetization. Because there was no intermediate blocking SiO_2 layer between porous Fe_3O_4 cores and dual-porous SiO_2 shells, continues and highly accessible mesopores from SiO_2 shell to Fe_3O_4 core can be achieved, which endows the microspheres with high surface area (426 $m^2\ g^{-1}$) and large pore volume (0.48 $cm^3\ g^{-1}$). The unique triple-porous structure is believed to be favourable for hosting molecules of various sizes and shapes. Drug loading and release test indicated that the microspheres show high drug loading capacity and typical long sustained release properties with 5-fluorouracil (5-FU) as the model drug. Measurements of AC magnetic-field-induced heating properties showed that the obtained microsphere possesses high heating efficiency and is suitable as a hyperthermia agent for thermal therapy. And most interestingly, it is found that the drug release behaviour can be controlled or triggered by an external AC magnetic-field. With excellent biocompatibility and low cytotoxicity characterized *in vitro*, the obtained triple-porous Fe_3O_4@SiO_2 microspheres can be potentially used in the multiple biomedical therapies.

Experimental

Materials

$FeCl_3 \cdot 6H_2O$, NaAc, NaOH, ethylene glycol (EG), diethylene glycol (DEG), anhydrous ethanol, aqueous ammonia solution (28%), tetraethyl orthosilicate (TEOS, 98%), polyethylene glycol (PEG, $M_w = 20\,000$), sodium polyacrylate (PAAS, $M_w = 10\,000$), cetyltrimethylammonium bromide (CTAB), PVP were purchased from Shanghai Chemical Reagents Company (China) and used as received. Fluorinated pyrimidine 5-fluorouracil (5-FU) was purchased from Sigma-Aldrich (China, mainland). Deionized water was used in all experiments. Human blood plasma, human gastric cancer SGC-7901 cells and phosphate buffer saline (PBS) solutions were provided by Xi'an Fourth Military Medical University (China).

Synthesis of mesoporous Fe_3O_4 microspheres

Mesoporous Fe_3O_4 microspheres were fabricated according a modified procedure.[39–41] Briefly, $FeCl_3 \cdot 6H_2O$ (1.35 g), NaAc (3.60 g), PEG (0.5 g), and PAAS (0.2 g) were dissolved in mixture of EG and DEG (40 mL) to form a homogeneous solution with vigorously stirring. This solution was transferred into a Teflon-lined stainless autoclave (50 mL capacity), and sealed heating at 200 °C. After reaction for 12 h, the autoclave was cooled to room temperature naturally. The precipitate was collected by magnetic separation and washed several times under sonication with water and ethanol and then dried under vacuum at 40 °C.

Synthesis of triple-porous m-Fe_3O_4@dm-SiO_2 microspheres

Dual-porous SiO_2 shells on mesoporous Fe_3O_4 cores were obtained through a novel "surfactant-templating and surface-protected etching" strategy by controlling the permeation of silica shells. Here, CTAB was used as surfactant template and PVP was as surface protecting agent. Firstly, 0.10 g of as-prepared m-Fe_3O_4 particles were treated with 0.1 M HCl aqueous solution (50 mL) by ultrasonication. After the treatment for 10 min, the m-Fe_3O_4 particles were separated and rinsed several times with deionized water, and homogeneously dispersed into the solution of CTAB (0.02 M, 50 mL) by

 This journal is © The Royal Society of Chemistry 2017

Open Access Article. Published on 22 June 2017. Downloaded on 1/24/2026 4:51:22 AM.
This article is licensed under a Creative Commons Attribution 3.0 Unported Licence.

mechanical stirring for 20 min. The mixture was diluted with water (30 mL) and ethanol (60 mL), and homogenized under ultrasonic conditions for 30 min, prior to the addition of an ammonia solution (1.2 mL). And then, 0.5 mL of TEOS was added dropwise for 30 min. The resultant mixture was stirred continuously for another 10 h at room temperature. Subsequently, the solution was stayed still at 8 °C for 1 h and the m-Fe_3O_4@CTAB/SiO_2 microspheres were obtained. Secondly, as-prepared m-Fe_3O_4@CTAB/SiO_2 particles were washed and redispersed in deionized water (30 mL) and were heat-treated in water at 98 °C by mechanical stirring for 2–3 h in the presence of PVP (0.5 g, $M_w \sim 50\,000$). The mixture was cooled to room temperature rapidly. In this process, the silica coating slowly becomes porous upon hot-water etching with the cooperative effects of CTAB and PVP. The black m-Fe_3O_4@dm-SiO_2 particles were washed repeatedly with deionized water, dried under vacuum, and stored in a freezer before characterization and usage.

Characterization

The crystal structure and purity of the resulting products were examined by powder X-ray diffraction (XRD) analysis using Cu K_α radiation. Morphologies of the samples were studied using field emission scanning electron microscopy (FE-SEM, JSM-7000F). Transmission electron microscopic (TEM) images, and selected area electron diffraction (SAED) patterns were obtained on a JEOL JEM-2010 microscope. Magnetic properties (*M–H* curve and *M–T* curve) of the products were investigated using a Lake Shore vibrating sample magnetometer (VSM) with a maximum applied magnetic field of 10 kOe. The BET surface areas of the samples analyzed by nitrogen adsorption–desorption isotherm measurements were carried out on a Micromeritics ASAP 2020 instrument. The Brunauer–Emmett–Teller (BET) surface area and the pore size distribution plots were calculated by applying the linear part of the BET plot and the Barrett–Joyner–Halenda (BJH) model, respectively.

Zeta potentials were measured by using a Malvern Instrument ZetaSizer Nano ZS90 at temperature of 25 °C.

Plasma stability

Blank m-Fe_3O_4@dm-SiO_2 microspheres were incubated with human blood plasma in centrifuge tubes for 24 h under mild shaking and then separated by a magnet. The sample was washed once with water and then re-dispersed in water. The size of the colloidal particles was determined with Dynamic Light Scattering (DLS) with a Malvern Instrument ZetaSizer Nano ZS90.

Hyperthermia

To evaluate the *in vitro* inductive heating property of the m-Fe_3O_4@dm-SiO_2 microspheres, time-dependent calorimetric experiments were conducted by exposing 5 mL of the colloid, held in a clear glass biological test tube, to 55 kHz AC magnetic fields. The temperature of AC magnetic field generator was controlled by cycling cooling water at 25 °C. The coil of the AC magnetic field has 5 loops, and the strength of the magnetic field (H) is 4.5 kA m^{-1}. The m-Fe_3O_4@dm-SiO_2 microspheres were dispersed in physiological saline with the concentration of 5, 7.5, 10 mg mL^{-1} and treated with ultrasound for 30 min before the measurements. The heat generated by the samples was investigated by measuring the change in temperature of the solution as a function of time using a thermometer.

Drug loading and *in vitro* release from m-Fe_3O_4@dm-SiO_2 microspheres

5-FU was used as a model drug to assess the drug loading and release behaviour of the m-Fe_3O_4@dm-SiO_2 microspheres. The loading of 5-FU was carried out by soaking microspheres in a concentrated 5-FU solution while stirring to ensure the diffusion of drug molecules into the mesopores. Briefly, 300 mg of m-Fe_3O_4@dm-SiO_2 microspheres was dispersed in 60 mL of drug solution containing 60 mg of 5-FU at room temperature. The mixture was then stirred for 24 h at room temperature to allow penetration of 5-FU molecules through porous shell channels and into the porous interiors of m-Fe_3O_4@dm-SiO_2 microspheres. To determine the loading profile of 5-FU, the mixture was magnetically separated and 0.5 mL of the supernatant was extracted from the vial at intervals of 0, 8, 16 and 24 h and analyzed by UV-vis spectroscopy at a wavelength of 266 nm. The 5-FU loading in the microspheres was calculated by subtracting the amount of 5-FU in the supernatant from the amount in the original drug solution.

The release profiles of 5-FU from m-Fe_3O_4@dm-SiO_2/5-FU particles were obtained as follows: first, 100 mg 5-FU-loaded microspheres were immersed in 20 mL of phosphate buffer saline (PBS) solutions at pH 7.4 and the mixtures were gently stirred at 37 °C. At predetermined time intervals, the dispersed particles were magnetically separated, and 500 μL of the released supernatant medium was extracted from solution. Meanwhile preheated fresh buffer (500 μL) was added to the original supernatant medium after each sampling. The extracted clear solution without magnetic particles was then diluted to 5 mL and analyzed by UV-vis spectroscopy at a wavelength of 266 nm to determine the concentration of 5-FU released from the microspheres. In addition, in order to investigate the magnetically controlled drug release behaviour of the m-Fe_3O_4@dm-SiO_2/5-FU, an AC magnetic field of 55 kHz (the strength of the magnetic field was 4.5 kA m^{-1}) was applied to the solution in different stages of drug release.

In vitro cytotoxicity tests of the m-Fe_3O_4@dm-SiO_2 microspheres

To evaluate the cytotoxicity of m-Fe_3O_4@dm-SiO_2 microspheres, the human gastric carcinoma cells (SGC-7901) were used for the cell viability test. First, the cells were seeded into a 96 well flat-bottom microassay plate and cultured for 24 h. Then, m-Fe_3O_4@dm-SiO_2 samples with different concentrations (0, 8, 32, 64, 100 and 200 μg mL^{-1}) were added into wells, and were co-cultured with cells for 24 h. Cell viability was quantified by the 3-(4,5-dimethylthiazol-2-yl)-2,5-diphenyltetrazolium bromide (MTT) assay by using tissue culture plate as control sample.

Open Access Article. Published on 22 June 2017. Downloaded on 1/24/2026 4:51:22 AM.
This article is licensed under a Creative Commons Attribution 3.0 Unported Licence.

Results and discussion

The fabrication and controlled release procedure for the m-Fe_3O_4@dm-SiO_2 microspheres are schematically illustrated in Scheme 1. In the first step, Fe_3O_4 primary nanocrystals were synthesized through a hydrothermal reaction with the assistance of PEG and PAAS. To reduce the surface energy of nanocrystals, the primary nanoparticles assembled together to form hierarchical Fe_3O_4 porous microspheres. In the next step, mesoporous silica shells were deposited on the Fe_3O_4 microspheres by utilizing CTAB as the organic template. Subsequently, PVP was used as the surface protecting agent and adsorbed onto the surfaces of m-Fe_3O_4@CTAB/SiO_2 microspheres. Finally, under the surface protection of PVP, the CTAB template was removed and silica shells were gradually etched in a mild way by hot-water etching to realize the formation of dual-porous SiO_2 shells, resulting in triple-porous m-Fe_3O_4@dm-SiO_2 microspheres. When an alternating magnetic field was applied, as-prepared triple-porous microspheres can generate heat for hyperthermia, and the loaded drugs could be simultaneously released by field-controlled manners.

The morphology and structure of as-prepared m-Fe_3O_4 and m-Fe_3O_4@dm-SiO_2 microspheres were investigated by SEM and TEM analysis, as shown in Fig. 1. The representative SEM image of Fe_3O_4 microspheres (Fig. 1a) shows that the Fe_3O_4 particles are monodisperse and uniform on a large scale. The average size of the Fe_3O_4 particles is ~260 nm in diameter. The rough surface morphology and loose structure reveal that as-prepared Fe_3O_4 particles possess hierarchical structure, in which tiny Fe_3O_4 primary nanocrystals (~20 nm) assemble together to form Fe_3O_4 microspheres. Furthermore, from the SEM image (inset in Fig. 1a) and TEM image (Fig. 1b), the Fe_3O_4 microspheres have porous and hollow interior structure. The SAED pattern recorded on a single isolated microsphere reveals the crystalline nature of the material (inset in Fig. 1c). The crystal lattice fringes seen in HRTEM image (Fig. 1c) indicate that the microspheres are formed by geometrically random but lattice oriented attachment of smaller nanocrystals. The measured *d* spacing is 0.243 nm, which is in good agreement with the values for (222) planes of a cubic magnetite phase. The formation of mesoporous structure of Fe_3O_4 microspheres is believed to be due to the steric effect of PEG and PAAS. In this process, PEG and PAAS act as surfactant agent to prevent primary nanocrystals from close contacting and play an important role in the formation of loose and mesoporous structure.

Through a modified Stöber approach by using CTAB as template, core@shell structured m-Fe_3O_4@CTAB/SiO_2 microspheres were obtained (Fig. S1†). With the surface protection of PVP, the CTAB template was extracted and silica shells were selectively etched gradually by hot water so that dual-porous SiO_2 shells were achieved. The morphology of the mesoporous magnetic microspheres is clearly shown in SEM (Fig. 1d) and TEM image (Fig. 1e). It is worth noting that as-prepared SiO_2 shells possess dual-porous structure, in which perpendicular aligned mesochannels coexist with randomly distributed pores. This is significantly different from traditional mesoporous structures. This dual-porous shell structure can be more clearly observed in the magnified TEM image (Fig. 1f). Moreover, the size of the randomly distributed pores is markedly larger than that of perpendicular aligned mesochannels, which endows the mesoporous structure with great possibilities for holding different drugs with various sizes of molecules. In addition, unlike sandwich structured mesoporous silica microspheres,[42,43] as-prepared m-Fe_3O_4@dm-SiO_2 particles have no middle nonporous silica layer between Fe_3O_4 cores and mesoporous SiO_2 shells, and the pores of mesoporous SiO_2 directly connect with those of mesoporous Fe_3O_4 cores. This novel triple-porous structure is favourable for drug molecules to pass

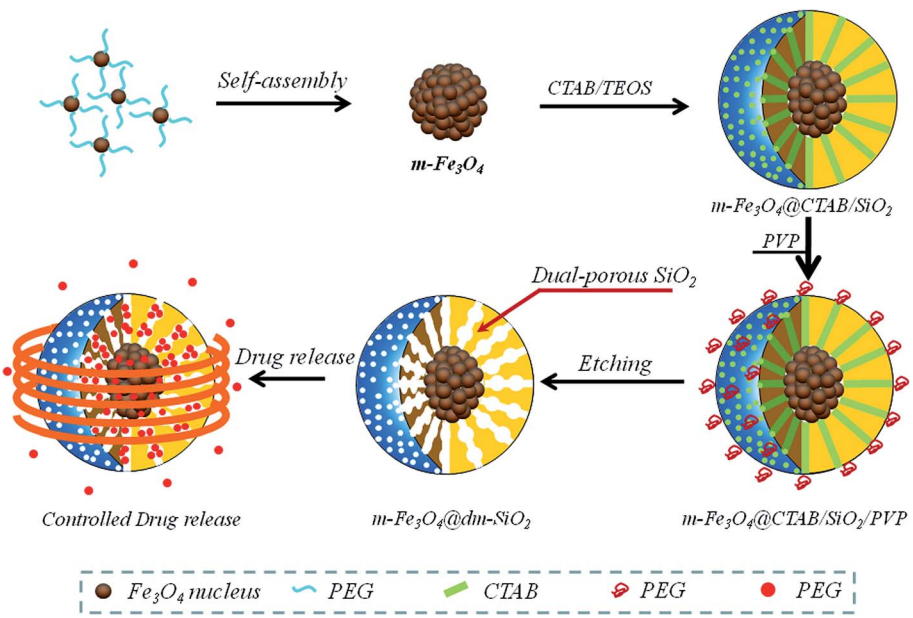

Scheme 1 Fabrication strategy and controlled-release procedure for the m-Fe_3O_4@dm-SiO_2 microspheres.

 This journal is © The Royal Society of Chemistry 2017

Open Access Article. Published on 22 June 2017. Downloaded on 1/24/2026 4:51:22 AM.
This article is licensed under a Creative Commons Attribution 3.0 Unported Licence.

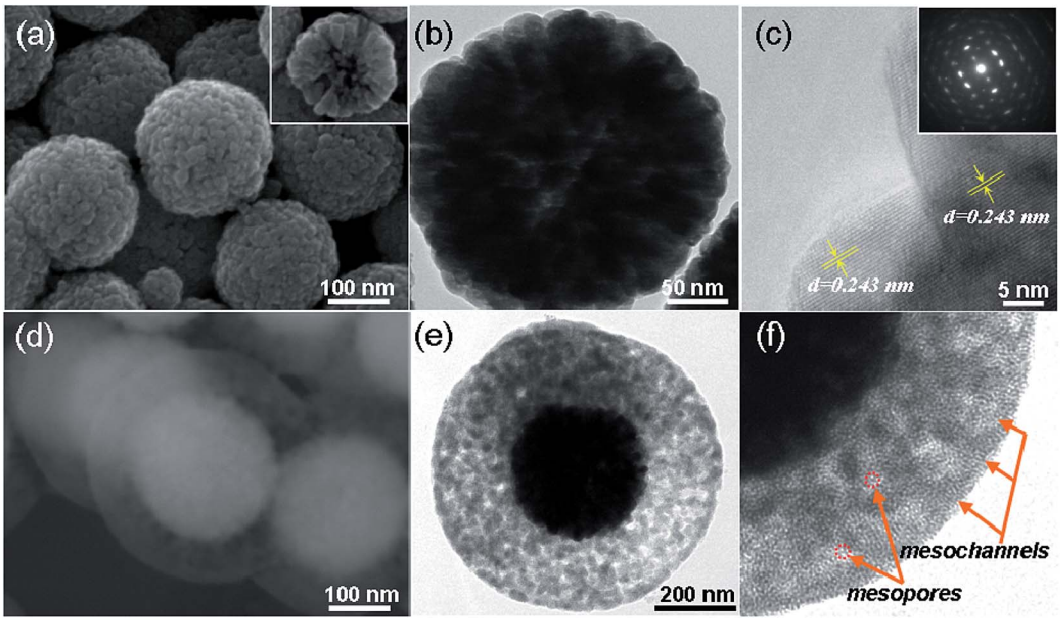

Fig. 1 (a) SEM image and (b) TEM image of m-Fe_3O_4 particles, (c) HRTEM image and SAED pattern of m-Fe_3O_4 particles (the inset), (d) SEM and (e) TEM image of m-Fe_3O_4@dm-SiO_2 mesoporous microspheres, (f) magnified TEM image of dual-porous structure in silica shell.

through the dual porous SiO_2 shells and enter the mesoporous interior of Fe_3O_4 cores, thus helps to enhance the drug loading capacity and achieve desirable sustainable drug release performance. The formation of this dual-porous structure in SiO_2 shells is believed to be due to the cooperative effect of CTAB and PVP. In SiO_2 coating process, CTAB templates interact with the silica oligomers *via* Coulomb forces, and both of them cooperatively assemble on the surface of Fe_3O_4 microspheres to form ordered mesostructure. The perpendicular aligned orientation of mesochannels may result from the preferable alignment fashion of the rod-shaped silicate/CTAB complexes on the surface of the Fe_3O_4 microspheres. On the other hand, the presence of PVP on the surface dramatically increases the stability of silica against etching by hot water because of the strong hydrogen bonds formed between its carbonyl groups and the hydroxyls on the silica surface. Prior studies have found that the dissolution of colloidal silica in water proceeds by breaking the Si–O–Si network structures. The etching efficiency is directly related to the degree of condensation of the silica network. Regions with perfect Si–O–Si networks are more resistant to water etching, while those with highly discontinuous networks can be dissolved quickly. This is the reason why randomly distributed pores can be formed after controlled water etching. From Fig. 2, it can be seen that the size of pores can be tuned by

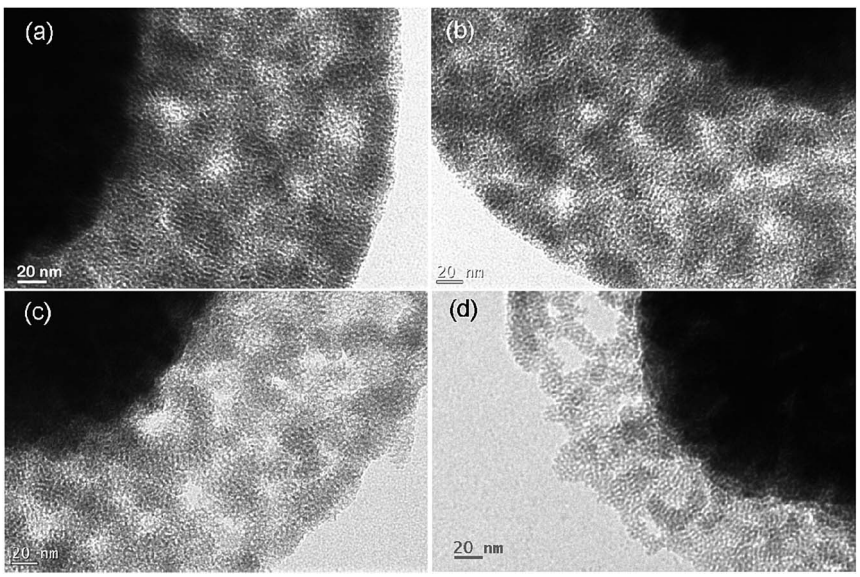

Fig. 2 TEM images of dual-porous silica shells obtained at different etching time: (a) 2 h, (b) 2.5 h, (c) 3 h, (d) 4 h.

Open Access Article. Published on 22 June 2017. Downloaded on 1/24/2026 4:51:22 AM.
This article is licensed under a Creative Commons Attribution 3.0 Unported Licence.

changing the etching time. When the etching time was prolonged from 2 h to 4 h, the randomly distributed pores become larger and larger.

Fig. 3 shows the XRD patterns of as-prepared m-Fe_3O_4 and m-Fe_3O_4@dm-SiO_2 microspheres. All of the diffraction peaks can be well indexed to the magnetic cubic inverse spinel Fe_3O_4 (JCPDS 75-0033). No crystalline SiO_2 can be detected in sample of m-Fe_3O_4@dm-SiO_2 microspheres. The average crystal size of the Fe_3O_4 cores, obtained by calculation of Sherrer's formula, is about 20 nm, which is consistent with the SEM and TEM images (Fig. 1a and b). The XRD results of m-Fe_3O_4@dm-SiO_2 microspheres suggest that Fe_3O_4 as the cores of m-Fe_3O_4@dm-SiO_2 microspheres are stable during the silica coating and hot-water etching.

To better understand the resulting porous structures, nitrogen adsorption–desorption measurements were carried out. Fig. 4 shows the representative N_2 adsorption–desorption isotherms and the corresponding pore size distributions of the m-Fe_3O_4@dm-SiO_2 samples. The N_2 adsorption–desorption isotherms exhibit typical type-IV curve, revealing the presence of mesoporous structure. Moreover, it can be clearly seen that three peaks, located at around 2.5 nm, 4 nm and 10.5 nm respectively, appear on the pore size distribution curve (Fig. 4 inset), indicating that as-prepared microspheres possess triple-porous structure. Obviously, the peaks centered at 2.1 nm and 4 nm should be attributed to the perpendicular aligned mesochannels and randomly distributed pores in silica shell respectively and other weaker signal centered at 10.5 nm is corresponded to the porous Fe_3O_4 core. The BET (Brunauer–Emmett–Teller) surface area and total pore volume of m-Fe_3O_4@dm-SiO_2 microspheres were calculated to be 426 $m^2\ g^{-1}$ and 0.48 $cm^3\ g^{-1}$, respectively. Because of the large surface area, large pore volume, and novel triple-porous structures, the m-Fe_3O_4@dm-SiO_2 microspheres have potential to be used as efficient drug carriers. Drugs with various sizes of molecules could be absorbed and moved into the internal mesopores.

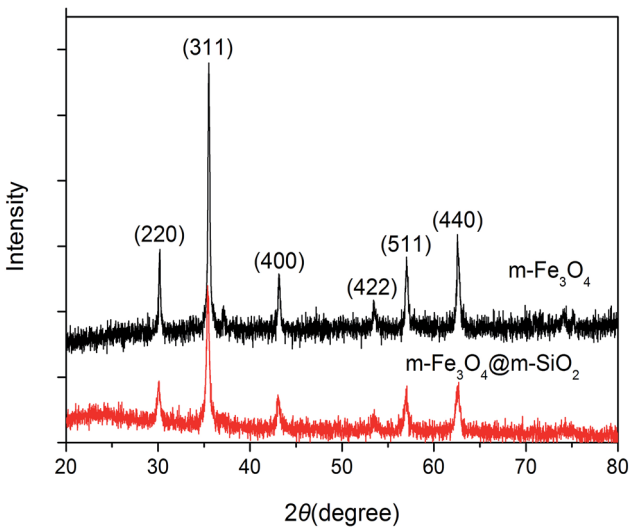

Fig. 3 The XRD patterns of m-Fe_3O_4 and m-Fe_3O_4@dm-SiO_2 microspheres.

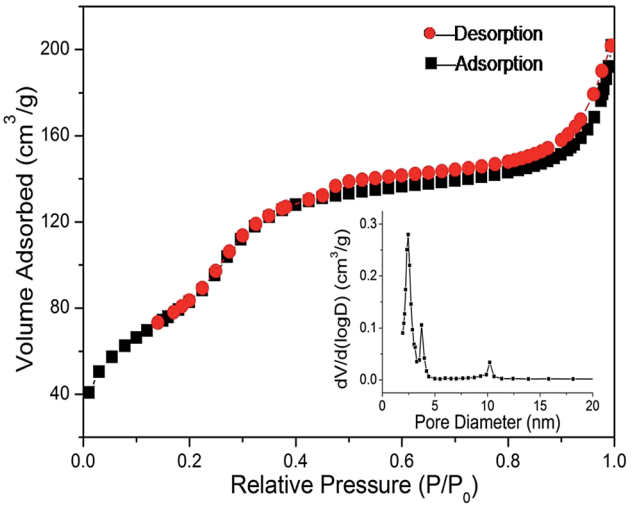

Fig. 4 N_2 adsorption–desorption isotherms and pore size distribution (the inset) of the synthesized m-Fe_3O_4@dm-SiO_2 microspheres. The adsorption branch is shown in black color and the desorption branch in red color.

The typical room temperature magnetization loops of m-Fe_3O_4 and m-Fe_3O_4@dm-SiO_2 microspheres were depicted in Fig. 5. The results show the saturation magnetization of m-Fe_3O_4 and m-Fe_3O_4@dm-SiO_2 samples are 81 and 52 emu g^{-1}, respectively. No remanence and coercivity were detected for all of the samples, indicating superparamagnetic nature of particles. The lower value of magnetization for m-Fe_3O_4@dm-SiO_2 microspheres is due to the presence of nonmagnetic SiO_2 shell. The inset in Fig. 5 shows the typical magnetization *vs.* temperature plot of m-Fe_3O_4@dm-SiO_2 microspheres measured in an applied field of 500 Oe. The *M–T* curve shows that the Curie temperature (T_C) of m-Fe_3O_4@dm-SiO_2 is about 580 °C, which is

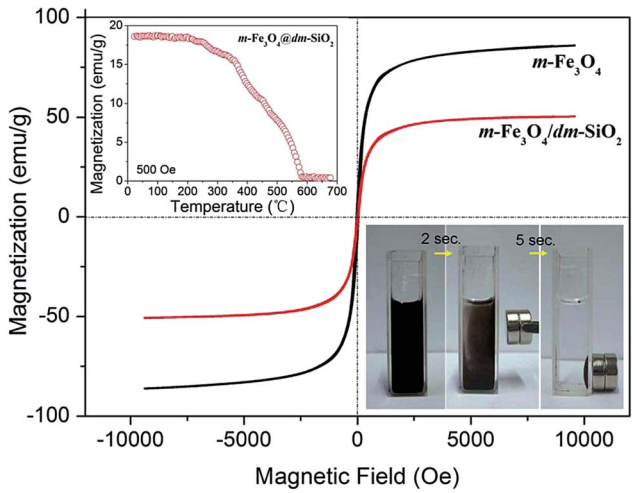

Fig. 5 Room temperature magnetization loops of m-Fe_3O_4 and m-Fe_3O_4@dm-SiO_2 microspheres. Insets show the magnetization *vs.* temperature plot of m-Fe_3O_4@dm-SiO_2 measured in an applied field of 500 Oe (upper left) and the photographs of an aqueous suspension of m-Fe_3O_4@dm-SiO_2 microspheres before and after magnetic capture within 5 s (bottom right).

This journal is © The Royal Society of Chemistry 2017

Open Access Article. Published on 22 June 2017. Downloaded on 1/24/2026 4:51:22 AM.
This article is licensed under a Creative Commons Attribution 3.0 Unported Licence.

in agreement with that reported for Fe_3O_4.[44] The microspheres show fast movement to the applied magnetic field and redisperse quickly with a slight shake once the magnetic field is removed (insets in Fig. 5), suggesting that the microspheres possess excellent magnetic responsivity and redispersibility. Furthermore, negligible precipitate was observed for the suspension within 24 hours, confirming the stability of the colloidal particles in aqueous suspension. The stability of the aqueous dispersion of the synthesized m-Fe_3O_4@dm-SiO_2 in aqueous medium was also verified from its measured zeta potential values, as seen from Fig. S2 and S3.† The initial zeta potential of m-Fe_3O_4@dm-SiO_2 was −37.4 mV and then stayed almost unchanged (∼−36.6 mV) after 30 days. The surface charge of colloidal particles is not only from the hydroxyl groups adsorbed on the surface, but also from the silanol groups formed by the breaking of the Si–O–Si bond during etching. The negatively charged surface provides the m-Fe_3O_4@dm-SiO_2 colloids with strong interparticle repulsions, which benefits their stability in aqueous solution.

We also examined the buffer stability of the nanosystems, and we found that the nanosystems were still well dispersed in phosphate buffer saline solutions after being stored 24 h. The aggregation and precipitation of the particles were not evident, indicating the nanosystems remained stable. Although the zeta potential was increased to −25.2 mV (Fig. S4†) due to the presence of cations, the remaining negative charge on the surface is still the main reason to ensure that the colloidal particles do not aggregate and precipitate in the buffer solution.

In order to meet the requirements of the *in vivo* use, the plasma stability of the nanosystems must be concerned. By monitoring the changes of mean hydrodynamic diameter (D_h) of colloidal particles in the plasma, we can determine whether the occurrence of protein adsorption or aggregation, and thus to evaluate its plasma stability. The results showed that the plasma treated nanosystems showed no obvious protein-induced size increase (or aggregation), as shown in Fig. S5,† indicating that the colloidal particles have the plasma stability and are potentially to act as drug carrier *in vivo* applications.

Fig. 6 represents the time-dependent temperature curves obtained after application of an AMF on m-Fe_3O_4@dm-SiO_2 suspensions. As seen in Fig. 6, after being exposed to the 55 kHz AMF (field strength is 4.5 kA m^{-1}) for 12 min, sufficient energy deposition was achieved, and the temperatures of physiological saline suspensions containing m-Fe_3O_4@dm-SiO_2 microspheres were increased to 41 °C, 48 °C and 56 °C when the colloidal concentrations are 5, 7.5, and 10 mg mL^{-1}, respectively. The heat generation involves several different mechanisms. For superparamagnetic iron-oxide nanoparticles, heat-generation under an AMF from eddy currents and hysteresis loop will be negligible.[45] Thus, it is believed that the heat generation are mainly attributed to Brownian relaxation modes (heat due to friction arising from total particle oscillations) and Neel relaxation modes (heat due to rotation of the magnetic moment with each field oscillation).[46] A reasonable assumption is that 5–10 mg of magnetic material concentrated in each cm^3 of tumor tissue is appropriate for magnetic hyperthermia in human patients.[47] From Fig. 6 it can be observed that, for

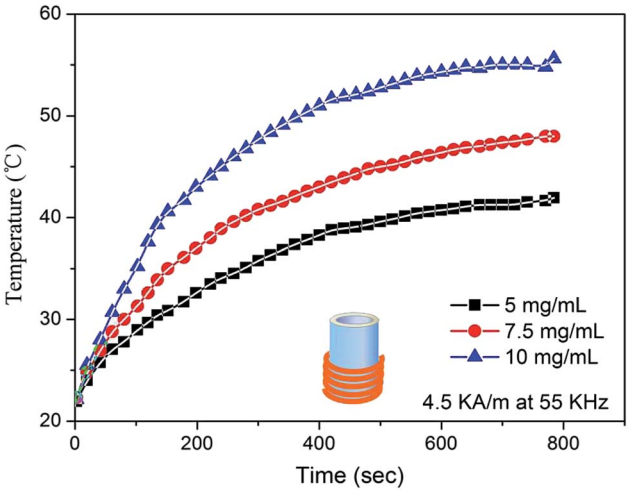

Fig. 6 Time-dependent heating curves acquired under AMF (55 kHz, 4.5 kA m^{-1}) for various concentrations of m-Fe_3O_4@dm-SiO_2 suspensions.

suspensions with concentration of 5–10 mg mL^{-1}, a hyperthermia temperature (41–56 °C) can be quickly achieved under AMF.

To investigate loading and release properties of m-Fe_3O_4@dm-SiO_2 microspheres, we used anti-cancer drug, 5-FU, as a model drug to introduce into m-Fe_3O_4@dm-SiO_2 microspheres. As the size of 5-FU molecules is very small (∼0.5 nm), the pores of m-Fe_3O_4@dm-SiO_2 microspheres (with the minimum size of 2.5 nm) are big enough for holding or transport of drug.[48] The drug loading process is believed to relies on the physical adsorption of 5-FU in the mesopores. The loading capacity of 5-FU in the m-Fe_3O_4@dm-SiO_2 microspheres, after 24 h in 2 mg mL^{-1} 5-FU solution, is calculated to be 62 μg mg^{-1} (as seen in Fig. S6†).

The *in vitro* release profile of 5-FU from the m-Fe_3O_4@dm-SiO_2 microspheres with and without the use of external AMF actuation are demonstrated in Fig. 7. Same amount of 5-FU loaded m-Fe_3O_4@dm-SiO_2 microspheres were used in PBS solution for all the drug-release experiments. Under the condition of no AMF actuation, it was found that the m-Fe_3O_4@dm-SiO_2/5-FU microspheres have typical sustained release property and about 40% of drug is released from the microspheres after 20 h. A small burst release is observed within the initial 0.5 h, which is indicative of the released drug adsorbed on the surface or in the shallow nanopores. This sustained release property can be attributed to the multiple-mesoporous structure of m-Fe_3O_4@dm-SiO_2 microspheres. Under the excitation of AMF, however, the release of 5-FU is greatly promoted and a big burst release was observed in the initial 2 h of release. The cumulative drug release under AMF exposure was about 1.8 times greater than that without the AMF stimulus. Moreover, it is interesting to realize that, when an external AMF was applied to the drug-loaded microspheres for 1 h and 2 h respectively after 3 h and 11 h of sustained release, a significant increase in the amount of drug release was observed. After then, the release profile restores to a slow profile. In other words, the drug release behaviours of microspheres can be changed from a steady-state,

Open Access Article. Published on 22 June 2017. Downloaded on 1/24/2026 4:51:22 AM.
This article is licensed under a Creative Commons Attribution 3.0 Unported Licence.

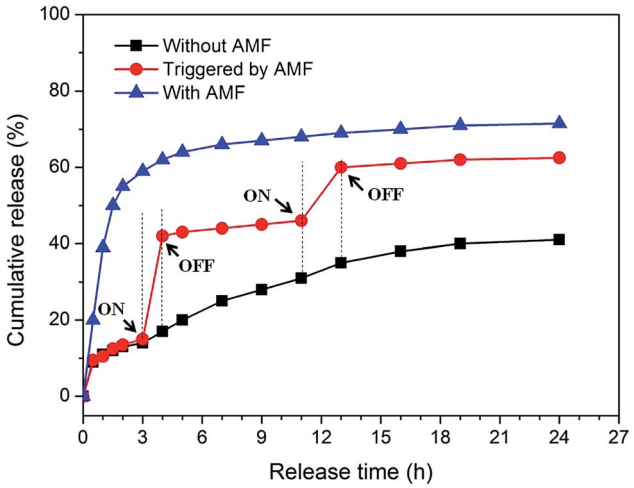

Fig. 7 Cumulative release of drug (5-FU) from m-Fe_3O_4@dm-SiO_2 microspheres without AMF stimulation (black squares), m-Fe_3O_4@dm-SiO_2 microspheres exposure to AMF (blue triangles), and m-Fe_3O_4@dm-SiO_2 microspheres with AMF stimulation applied after 3 h and 11 h of sustained release (red circles).

slow profile to a burst profile immediately after a short time exposure to the AMF stimuli. The plausible reason of this AMF actuated burst release is due to the thermal and dynamic energy produced by the AC magnetic field. High frequency magnetic-field can not only cause the oscillation or vibration of m-Fe_3O_4@dm-SiO_2/5-FU microspheres but also generate heat in magnetic microspheres. The vibration of m-Fe_3O_4@dm-SiO_2/5-FU microspheres and increase in temperature accelerate the diffusion of drug molecules from the interior mesopores of m-Fe_3O_4@dm-SiO_2 to the outside solution, thus resulted in the increase of drug release.

The *in vitro* cytotoxicity tests of m-Fe_3O_4@dm-SiO_2 microspheres with and without 5-FU loading were conducted using human gastric cancer SGC-7901 cells by a MTT assay, as shown in Fig. 8. The SGC-7901 cells were cultured with m-Fe_3O_4@dm-SiO_2 microspheres of varying concentrations for 24 h. The cytotoxicity was expressed by the percentage of cell viability compared to the control group. The result shows that the viability of the cells treated with m-Fe_3O_4@dm-SiO_2 microspheres without drug loading, in the concentration range of 8–200 μg mL^{-1}, remained above 80%, revealing that m-Fe_3O_4@dm-SiO_2 microspheres were of low cytotoxicity. On the contrary, for 5-FU loaded m-Fe_3O_4@dm-SiO_2 microspheres, the cell viability decreased obviously with increasing the concentration drug carriers. The cell viabilities were only 14% when the concentration of the sample was 200 μg mL^{-1}. The results can also be seen from microscopic images of cellular morphological changes (as seen in Fig. S14†).

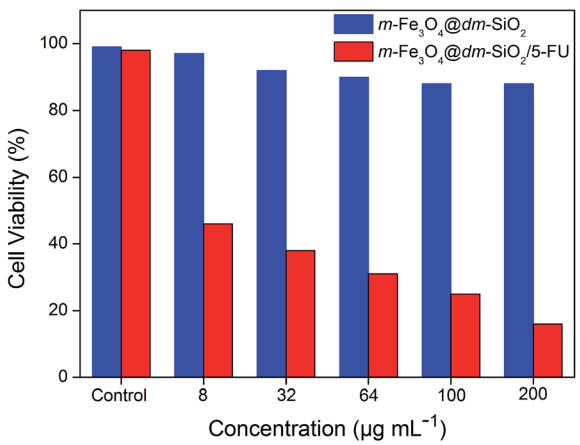

Fig. 8 Cell viability of SGC-7901 cells after being cultured at different concentrations of the m-Fe_3O_4@dm-SiO_2 (blue) and m-Fe_3O_4@dm-SiO_2/5-FU (red) for 24 h.

Conclusions

In conclusion, novel triple-porous m-Fe_3O_4@dm-SiO_2 microspheres were prepared *via* a controlled chemical process. The composite microsphere composes a mesoporous Fe_3O_4 core and a dual porous SiO_2 shell. With the cooperative effect of CTAB and PVP, a complex mesoporous structure, in which perpendicular aligned mesochannels accompanied with randomly distributed mesopores, can be achieved in the SiO_2 shell. As-prepared m-Fe_3O_4@dm-SiO_2 microspheres possess superparamagnetism, high magnetization (52 emu g^{-1}), high surface area (426 m^2 g^{-1}), large pore volume (0.48 cm^3 g^{-1}) and low cytotoxicity. The microspheres exhibit magnetic-field induced heating ability. Moreover, owning to the unique multiple-mesoporous structure, the m-Fe_3O_4@dm-SiO_2 microspheres show a high drug loading efficiency and typical sustained release property. Interestingly, as-prepared m-Fe_3O_4@dm-SiO_2 microspheres display AMF controlled drug release property. The drug release behaviours of microspheres can be changed from a steady-state, slow profile to a burst profile immediately after a short time exposure to the AMF stimuli. Therefore, as-prepared m-Fe_3O_4@dm-SiO_2 microspheres have great potential to be used in drug delivery and magnetic hyperthermia.

Acknowledgements

This work was supported by the National Natural Science Foundation (No. 51172178, 51501142) of P R China. The authors would like to acknowledge the support of Tangdu Hospital of The Fourth Military Medical University for offering assistance for this work.

Notes and references

1 J. P. Yang, D. K. Shen, L. Zhou, W. Li, X. M. Li, C. Yao, R. Wang, A. M. El-Toni, F. Zhang and D. Y. Zhao, *Chem. Mater.*, 2013, **25**, 3030–3037.
2 Y. Fang, G. F. Zheng, J. P. Yang, H. S. Tang, Y. F. Zhang, B. Kong, Y. Y. Lv, C. J. Xu, A. M. Asiri, J. Zi, F. Zhang and D. Y. Zhao, *Angew. Chem., Int. Ed.*, 2014, **53**, 5366–5370.
3 Y. Wang and H. C. Gu, *Adv. Mater.*, 2015, **27**, 576–585.

This journal is © The Royal Society of Chemistry 2017

Open Access Article. Published on 22 June 2017. Downloaded on 1/24/2026 4:51:22 AM.
This article is licensed under a Creative Commons Attribution 3.0 Unported Licence.

4 K. W. Qiu, Y. Lu, D. Y. Zhang, J. B. Cheng, L. Yan, J. Y. Xu, X. M. Liu, J. K. Kim and Y. S. Luo, *Nano Energy*, 2015, **11**, 687–696.
5 M. H. Wang, X. Q. Wang, Q. Yue, Y. Zhang, C. Wang, J. Chen, H. Q. Cai, H. L. Lu, A. A. Elzatahry, D. Y. Zhao and Y. H. Deng, *Chem. Mater.*, 2014, **26**, 3316–3321.
6 Y. P. Xie, Z. B. Yu, G. Liu, X. L. Ma and H. M. Cheng, *Energy Environ. Sci.*, 2014, **7**, 1895–1901.
7 K. P. Yuan, R. C. Che, Q. Cao, Z. K. Sun, Q. Yue and Y. H. Deng, *ACS Appl. Mater. Interfaces*, 2015, **7**, 5312–5319.
8 Y. F. Zhu, T. Ikoma, N. Hanagata and S. Kaskel, *Small*, 2010, **6**, 471–478.
9 E. Yu, I. Galiana, R. Martinez-Manez, P. Stroeve, M. D. Marcos, E. Aznar, F. Sancenon, J. R. Murguia and P. Amoros, *Colloids Surf., B*, 2015, **135**, 652–660.
10 Y. F. Zhu and C. L. Tao, *RSC Adv.*, 2015, **5**, 22365–22372.
11 M. E. de Sousa, M. B. F. van Raap, P. C. Rivas, P. M. Zelis, P. Girardin, G. A. Pasquevich, J. L. Alessandrini, D. Muraca and F. H. Sanchez, *J. Phys. Chem. C*, 2013, **117**, 5436–5445.
12 P. Guardia, R. Di Corato, L. Lartigue, C. Wilhelm, A. Espinosa, M. Garcia-Hernandez, F. Gazeau, L. Manna and T. Pellegrino, *ACS Nano*, 2012, **6**, 3080–3091.
13 L. Lartigue, C. Innocenti, T. Kalaivani, A. Awwad, M. D. S. Duque, Y. Guari, J. Larionova, C. Guerin, J. L. G. Montero, V. Barragan-Montero, P. Arosio, A. Lascialfari, D. Gatteschi and C. Sangregorio, *J. Am. Chem. Soc.*, 2011, **133**, 10459–10472.
14 B. Sivakumar, R. G. Aswathy, Y. Nagaoka, M. Suzuki, T. Fukuda, Y. Yoshida, T. Maekawa and D. N. Sakthikumar, *Langmuir*, 2013, **29**, 3453–3466.
15 F. Lu, A. Popa, S. W. Zhou, J. J. Zhu and A. C. S. Samia, *Chem. Commun.*, 2013, **49**, 11436–11438.
16 B. B. Shen, X. C. Gao, S. Y. Yu, Y. Ma and C. H. Ji, *CrystEngComm*, 2016, **18**, 1133–1138.
17 W. Guo, C. Y. Yang, H. M. Lin and F. Y. Qu, *Dalton Trans.*, 2014, **43**, 18056–18065.
18 C. L. Tao and Y. F. Zhu, *Dalton Trans.*, 2014, **43**, 15482–15490.
19 X. Yu and Y. F. Zhu, *Sci. Technol. Adv. Mater.*, 2016, **17**, 229–238.
20 C. S. S. R. Kumar and F. Mohammad, *Adv. Drug Delivery Rev.*, 2011, **63**, 789–808.
21 A.-H. Lu, E. L. Salabas and F. Schueth, *Angew. Chem., Int. Ed.*, 2007, **46**, 1222–1244.
22 Y.-W. Jun, J.-W. Seo and A. Cheon, *Acc. Chem. Res.*, 2008, **41**, 179–189.
23 J. Gao, H. Gu and B. Xu, *Acc. Chem. Res.*, 2009, **42**, 1097–1107.
24 J. Kim, J. E. Lee, J. Lee, J. H. Yu, B. C. Kim, K. An, Y. Hwang, C. H. Shin, J. G. Park and T. Hyeon, *J. Am. Chem. Soc.*, 2006, **128**, 688–689.
25 S. Giri, B. G. Trewyn, M. P. Stellmaker and V. S. Y. Lin, *Angew. Chem., Int. Ed.*, 2005, **44**, 5038–5044.
26 S. Huang, Y. Fan, Z. Cheng, D. Kong, P. Yang, Z. Quan, C. Zhang and J. Lin, *J. Phys. Chem. C*, 2009, **113**, 1775–1784.
27 Y. W. Jun, Y. M. Huh, J. S. Choi, J. H. Lee, H. T. Song, S. Kim, S. Yoon, K. S. Kim, J. S. Shin, J. S. Suh and J. Cheon, *J. Am. Chem. Soc.*, 2005, **127**, 5732–5733.
28 N. Bao, L. Shen, Y. Wang, P. Padhan and A. Gupta, *J. Am. Chem. Soc.*, 2007, **129**, 12374–12375.
29 C. Liu, B. S. Zou, A. J. Rondinone and J. Zhang, *J. Am. Chem. Soc.*, 2000, **122**, 6263–6267.
30 C. Liu and Z. J. Zhang, *Chem. Mater.*, 2001, **13**, 2092–2096.
31 N. Pinna, S. Grancharov, P. Beato, P. Bonville, M. Antonietti and M. Niederberger, *Chem. Mater.*, 2005, **17**, 3044–3049.
32 J. Liu, S. Z. Qiao, Q. H. Hu and G. Q. Lu, *Small*, 2011, **7**, 425–443.
33 Y. Zhu, T. Ikoma, N. Hanagata and S. Kaskel, *Small*, 2010, **6**, 471–478.
34 Q. Zhang, T. Zhang, J. Ge and Y. Yin, *Nano Lett.*, 2008, **8**, 2867–2871.
35 J. Ge, Q. Zhang, T. Zhang and Y. Yin, *Angew. Chem., Int. Ed.*, 2008, **47**, 8924–8928.
36 S.-h. Xuan, S.-F. Lee, J. T.-F. Lau, X. Zhu, Y.-X. J. Wang, F. Wang, J. M. Y. Lai, K. W. Y. Sham, P.-C. Lo, J. C. Yu, C. H. K. Cheng and K. C.-F. Leung, *ACS Appl. Mater. Interfaces*, 2012, **4**, 2033–2040.
37 L. Wu, H. Zhang, M. Wu, Y. Zhong, X. Liu and Z. Jiao, *Microporous Mesoporous Mater.*, 2016, **228**, 318–328.
38 F. Liu, J. Wang, Q. Cao, H. Deng, G. Shao, D. Y. B. Deng and W. Zhou, *Chem. Commun.*, 2015, **51**, 2357–2360.
39 S. Liu, R. Xing, F. Lu, R. K. Rana and J.-J. Zhu, *J. Phys. Chem. C*, 2009, **113**, 21042–21047.
40 H. Deng, X. L. Li, Q. Peng, X. Wang, J. P. Chen and Y. D. Li, *Angew. Chem., Int. Ed.*, 2005, **44**, 2782–2785.
41 B. Luo, X.-J. Song, F. Zhang, A. Xia, W.-L. Yang, J.-H. Hu and C.-C. Wang, *Langmuir*, 2010, **26**, 1674–1679.
42 Y. Deng, D. Qi, C. Deng, X. Zhang and D. Zhao, *J. Am. Chem. Soc.*, 2008, **130**, 28–29.
43 W. R. Zhao, J. L. Gu, L. X. Zhang, H. R. Chen and J. L. Shi, *J. Am. Chem. Soc.*, 2005, **127**, 8916–8917.
44 J. Wang, W. Wu, F. Zhao and G.-m. Zhao, *Appl. Phys. Lett.*, 2011, **98**, 083107.
45 R. Ghosh, L. Pradhan, Y. P. Devi, S. S. Meena, R. Tewari, A. Kumar, S. Sharma, N. S. Gajbhiye, R. K. Vatsa, B. N. Pandey and R. S. Ningthoujam, *J. Mater. Chem.*, 2011, **21**, 13388–13398.
46 S. Mornet, S. Vasseur, F. Grasset and E. Duguet, *J. Mater. Chem.*, 2004, **14**, 2161–2175.
47 Q. A. Pankhurst, J. Connolly, S. K. Jones and J. Dobson, *J. Phys. D: Appl. Phys.*, 2003, **36**, R167–R181.
48 G. L. Borosky and A. B. Pierini, *Org. Biomol. Chem.*, 2005, **3**, 649–653.